Supplementary Information for

An ultra-sensitive resistive pressure sensor based on hollow-sphere microstructure induced elasticity in conducting polymer film

Lijia Pan,[1,2†] Alex Chortos,[3†] Guihua Yu,[4] Yaqun Wang,[1] Scott Isaacson,[3] Ranulfo Allen,[2] Yi Shi,[1] Reinhold Dauskardt,[3] and Zhenan Bao[2]*

[1]Jiangsu Provincial Key Laboratory of Photonic and Electronic Materials, School of Electronic Science and Engineering, National Center of Microstructures and Quantum Manipulation, Nanjing University, Nanjing, 210093, China.
[2]Department of Chemical Engineering, Stanford University, Stanford, CA 94305, USA.
[3]Department of Materials Science and Engineering, Stanford University, Stanford, CA 94305, USA.
[4]Department of Mechanical Engineering and Materials Science and Engineering Program, The University of Texas at Austin, Austin, TX 78712, USA.

*To whom correspondence should be addressed. Email: zbao@stanford.edu.
[†]These authors contributed equally to this work.

Supplementary Figures

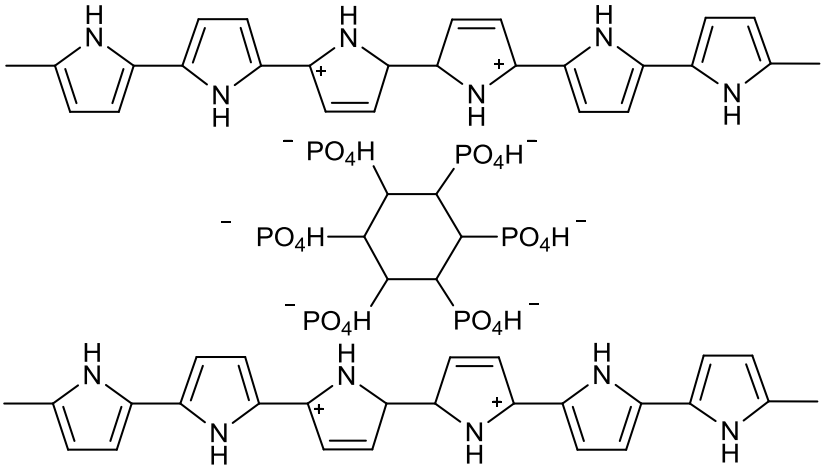

Supplementary Figure S1 | Schematic illustration of phytic acid doping and crosslinking PPy.

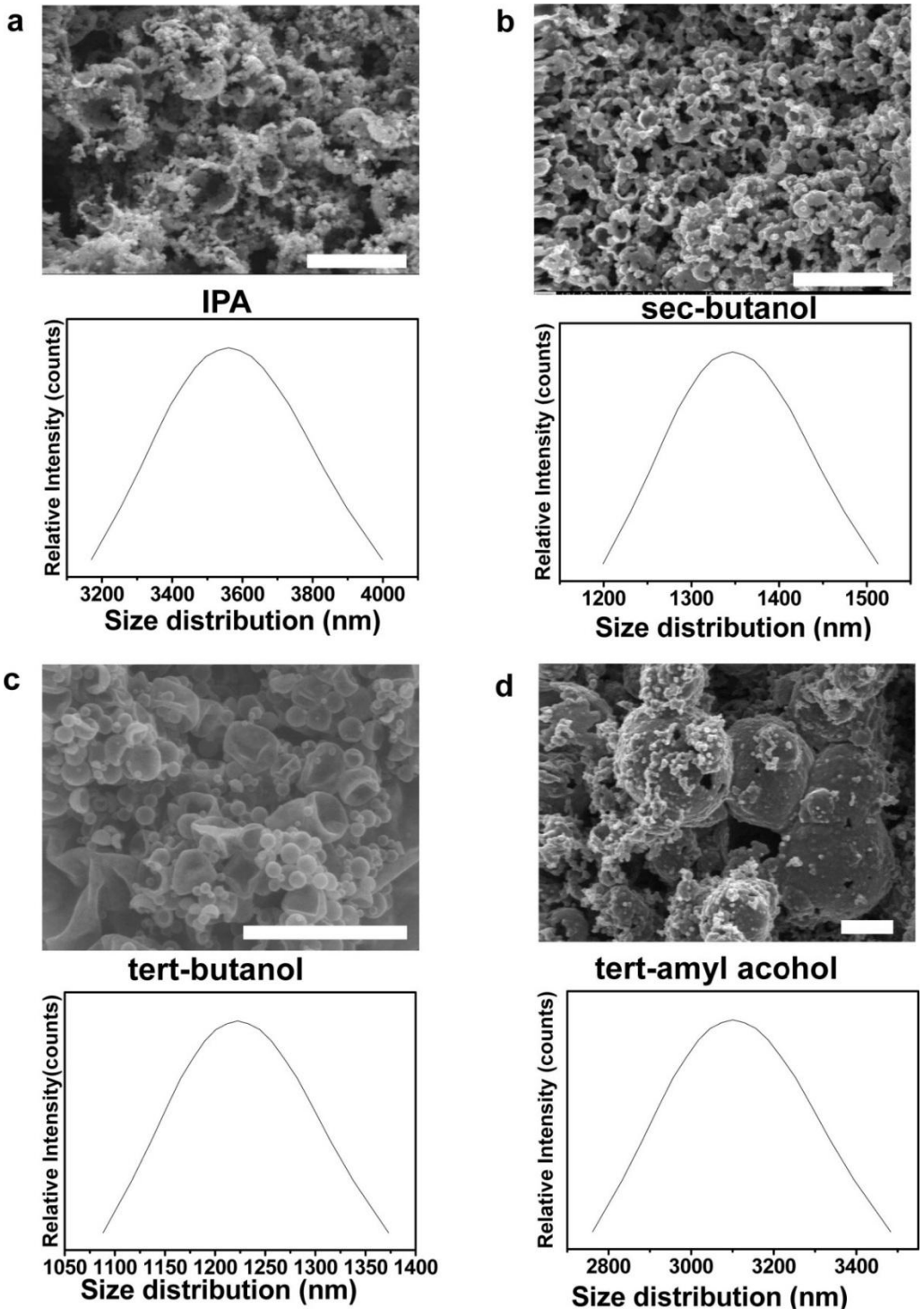

Supplementary Figure S2 | SEM images of microstructured PPy thin films and dynamic light scattering (DLS) measurements of their corresponding precursor solutions (without the initiator but with all other components kept constant). a, isopropanol. **b,** sec-butanol. **c,** tert-butanol. **d,** tert-amyl alcohol. The DLS results confirmed that phase separation occurred upon mixing the precursor solutions. Note that for the DLS measurement, no initiator was added to

solution A to allow for the measurement of the drop size in the mixed solution. The drop sizes were close to the final PPy particle size. The use of different solvents in solution B enabled control over the morphology of PPy.

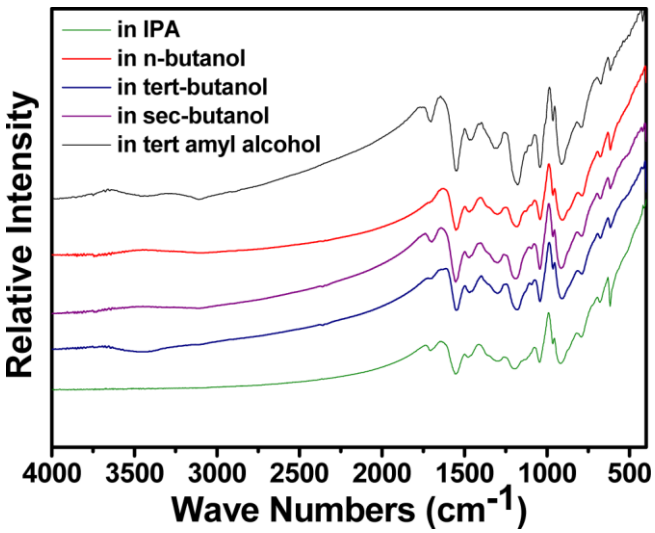

Supplementary Figure S3 | Fourier Transform infrared spectra (FTIR) of PPy samples synthesized using various solvents in solution B. The chemical structure of as-synthesized PPy was analyzed by FTIR spectroscopy and was found to be identical to that of typical PPy. The peak at approximately 1552 cm^{-1} corresponds to the characteristic peak of PPy and arises from the in-ring stretching vibrations of C=C and C-C bonds in the pyrrole rings and the stretching vibrations of C=C and C-N bonds[62]. The peak at approximately 1462 cm^{-1} was attributed to the stretching vibration of C-N. The peaks at 1300 cm^{-1} and 1200 cm^{-1} can be assigned to the C-N stretching vibration and C-C stretching vibration, respectively. The peak at approximately 1037 cm^{-1} was attributed to the C-H out-of-plane bending vibration. The peak at approximately 695 cm^{-1} corresponds to the C-H out-of-plane bending vibration mode.

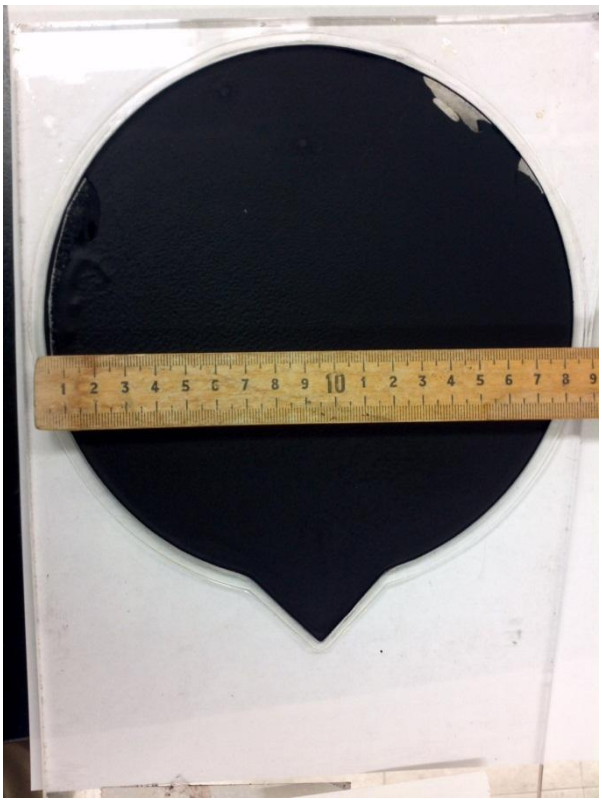

Supplementary Figure S4 | Large area fabrication of films. Films as large as 255 cm^2 have been fabricated. The standard deviation in the thickness was 24%, while the standard deviation in the density was 16%. The defects near the left and top right of the image were caused by removing the barrier that contained the material on the substrate.

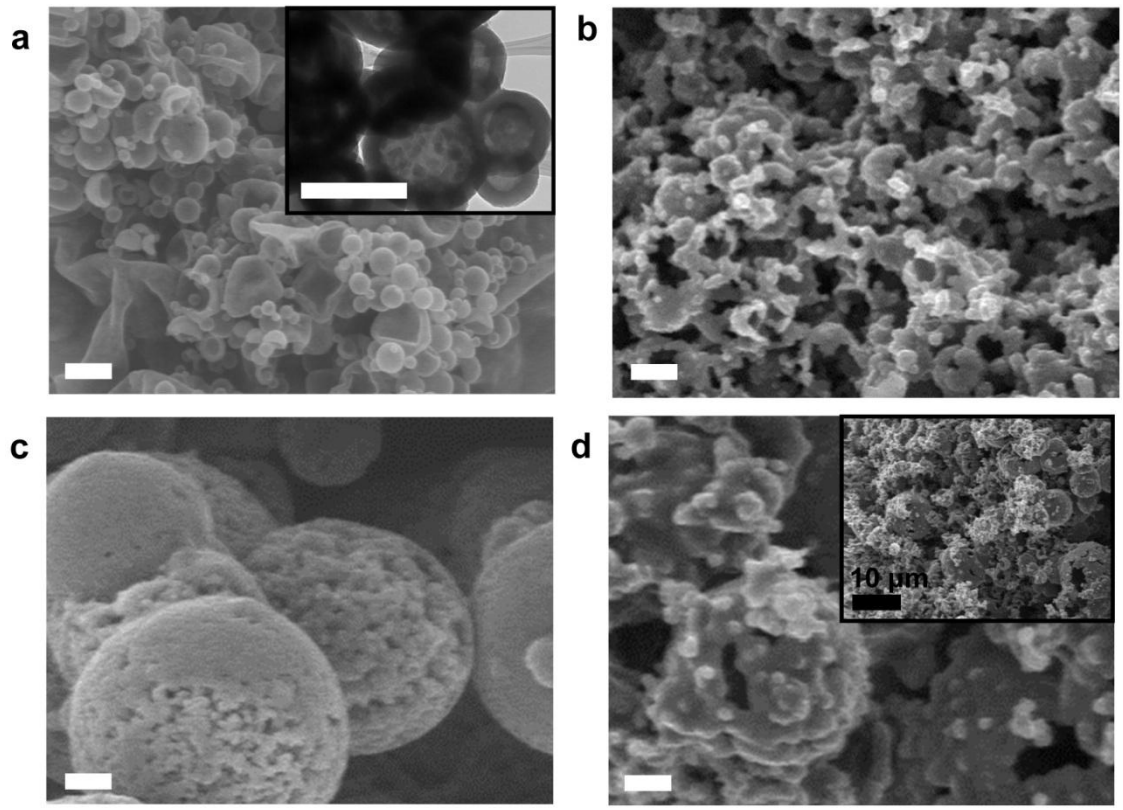

Supplementary Figure S5 | Using different solvents in solution B enabled control over the morphology of PPy hydrogels. a, tert-butanol (inset is the TEM image showing its hollow-sphere structures). **b,** sec-butanol. **c,** n-butanol (yielding solid-sphere structures). **d,** tert-amyl alcohol (inset, the overview SEM image). Scale bars: 1 μm.

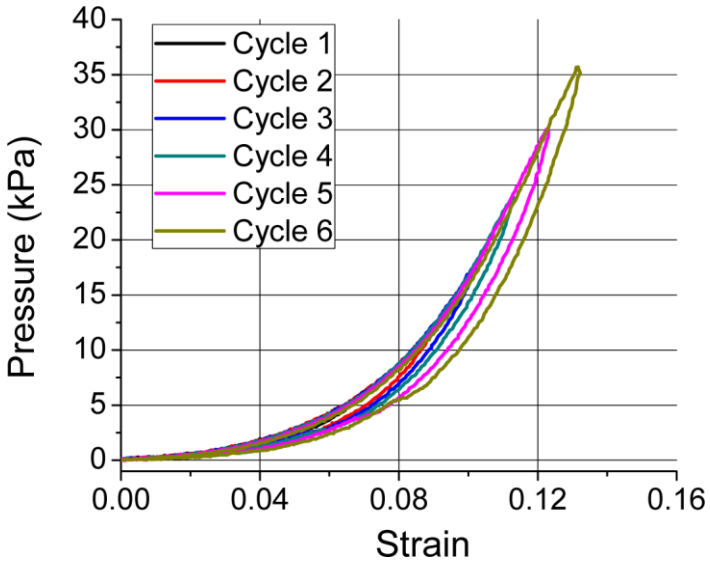

Supplementary Figure S6 | Investigation of mechanical hysteresis as a function of maximum applied strain. Pressure vs. strain curves for a PPy thin film with increasing maximum applied strain. The loading curves overlap, and the hysteresis increases with increasing applied pressure. The hysteresis was quantified as the maximum difference between the loading and unloading curves divided by the full-scale output.

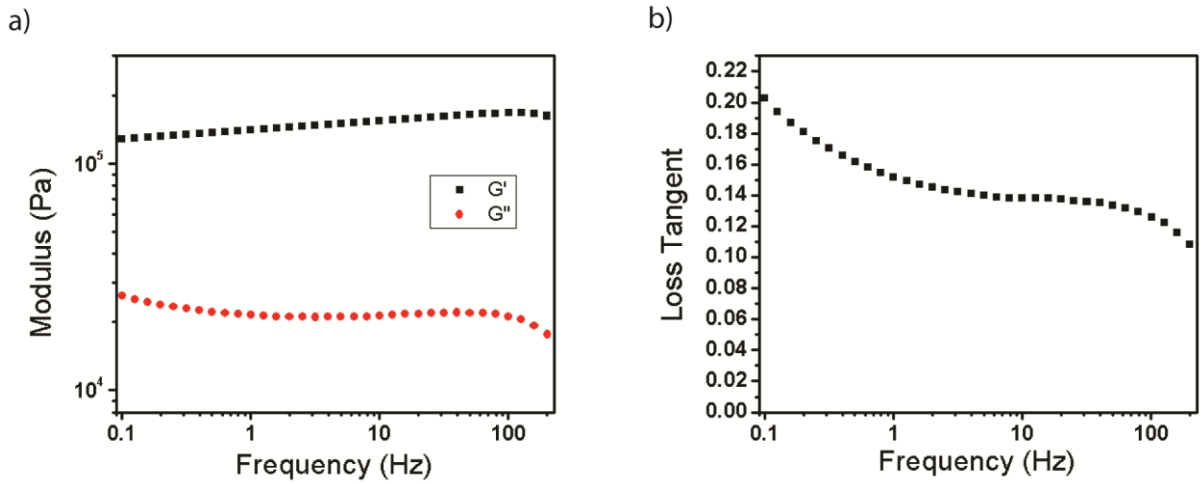

Supplementary Figure S7 | Dynamic frequency sweep of a dried hydrogel at a strain of 1% and at room temperature. **a**, storage and loss modulus. **b**, loss tangent.

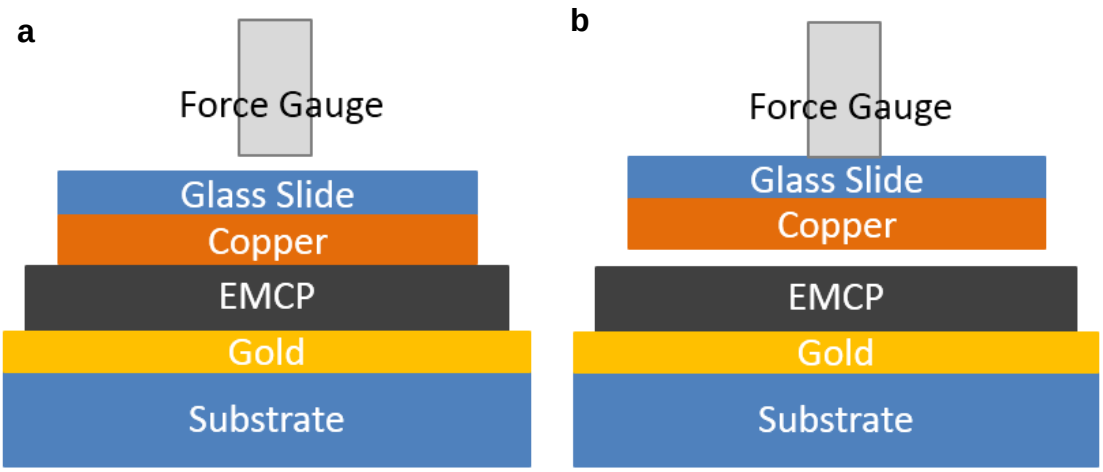

Supplementary Figure S8 | Diagram of methods for measuring the resistance vs pressure characteristics of the EMCP-electrode interface. a, Use of a copper electrode and glass slide placed on the EMCP surface. **b,** A top electrode and glass slide were attached to the force gauge and lowered onto the surface of the EMCP.

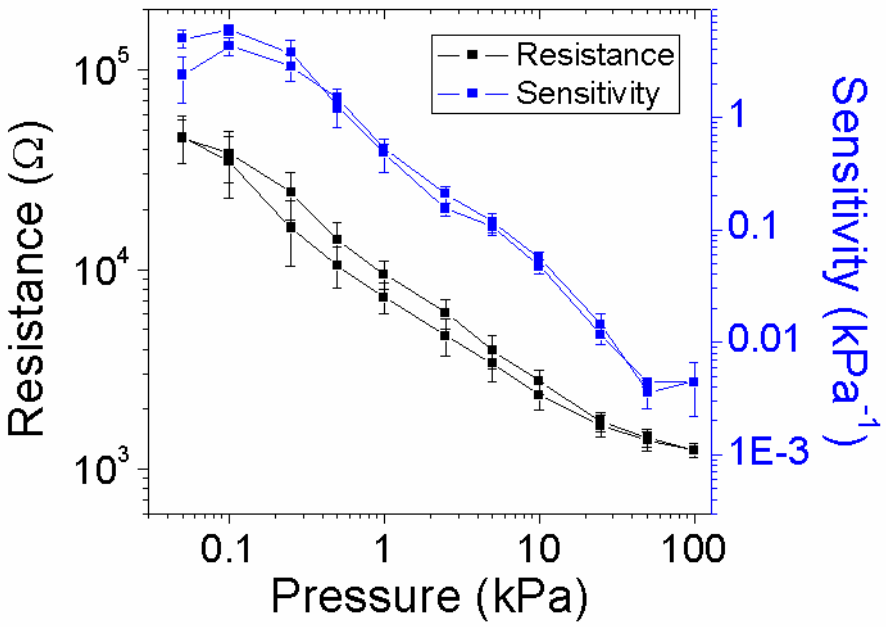

Supplementary Figure S9 | Resistance response and pressure sensitivity of the EMCP pressure sensor within the range of 0–100 kPa. The data was collected using the suspended–electrode structured device.

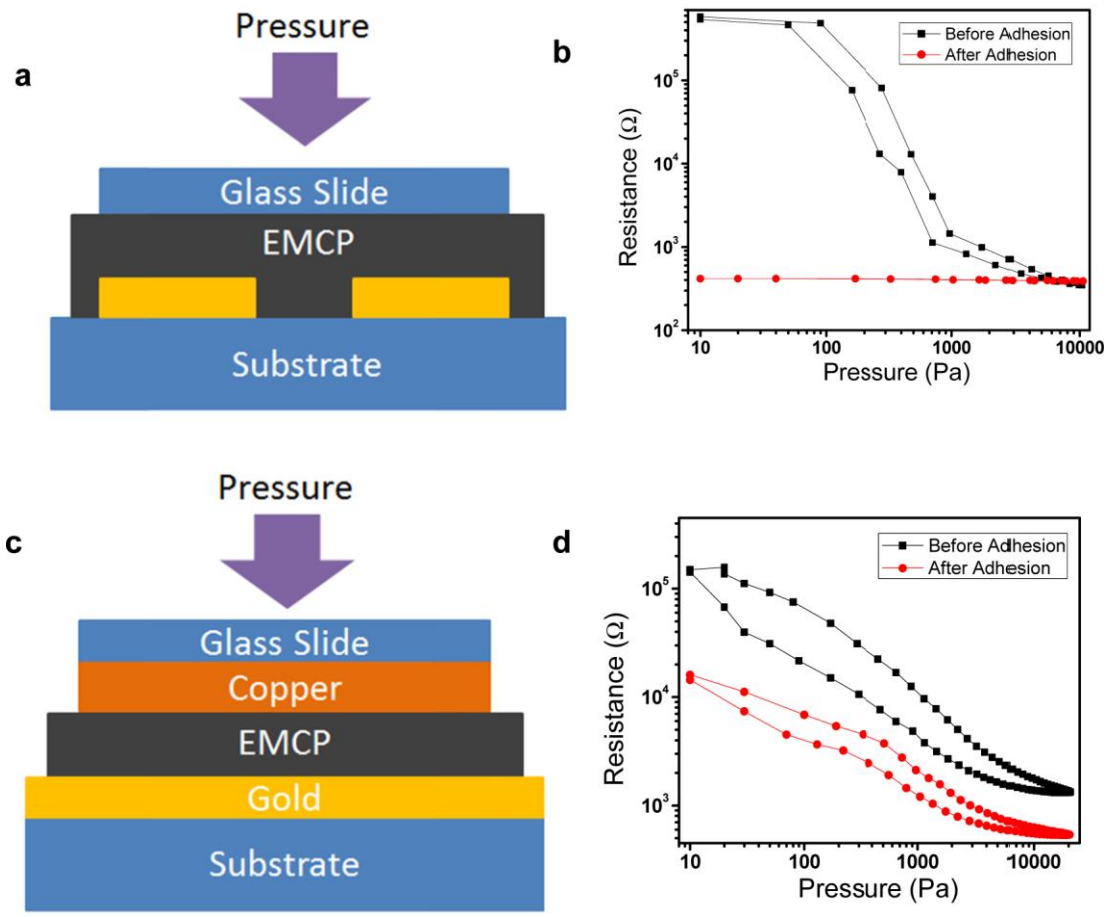

Supplementary Figure S10 | Effect of adhesion on sensing in bottom-contact devices. a, Diagram of the bottom-contact device structure. Gold electrodes were evaporated on a glass slide through a shadow mask. The microstructured PPy was placed on top of the electrodes, and a glass slide measuring 1 cm × 1 cm was used to define the area over which pressure was applied. **b,** Response of the bottom-contact device before and after adhesion of the microstructured PPy. Before adhesion, the device displayed a change in resistance with pressure on the same order of magnitude as the sandwich geometry. After adhesion to the electrodes, a negligible pressure response was observed. **c,** Diagram of the sandwich geometry. **d,** Pressure response of the EMCP before and after adhesion of the PPy to the gold electrode.

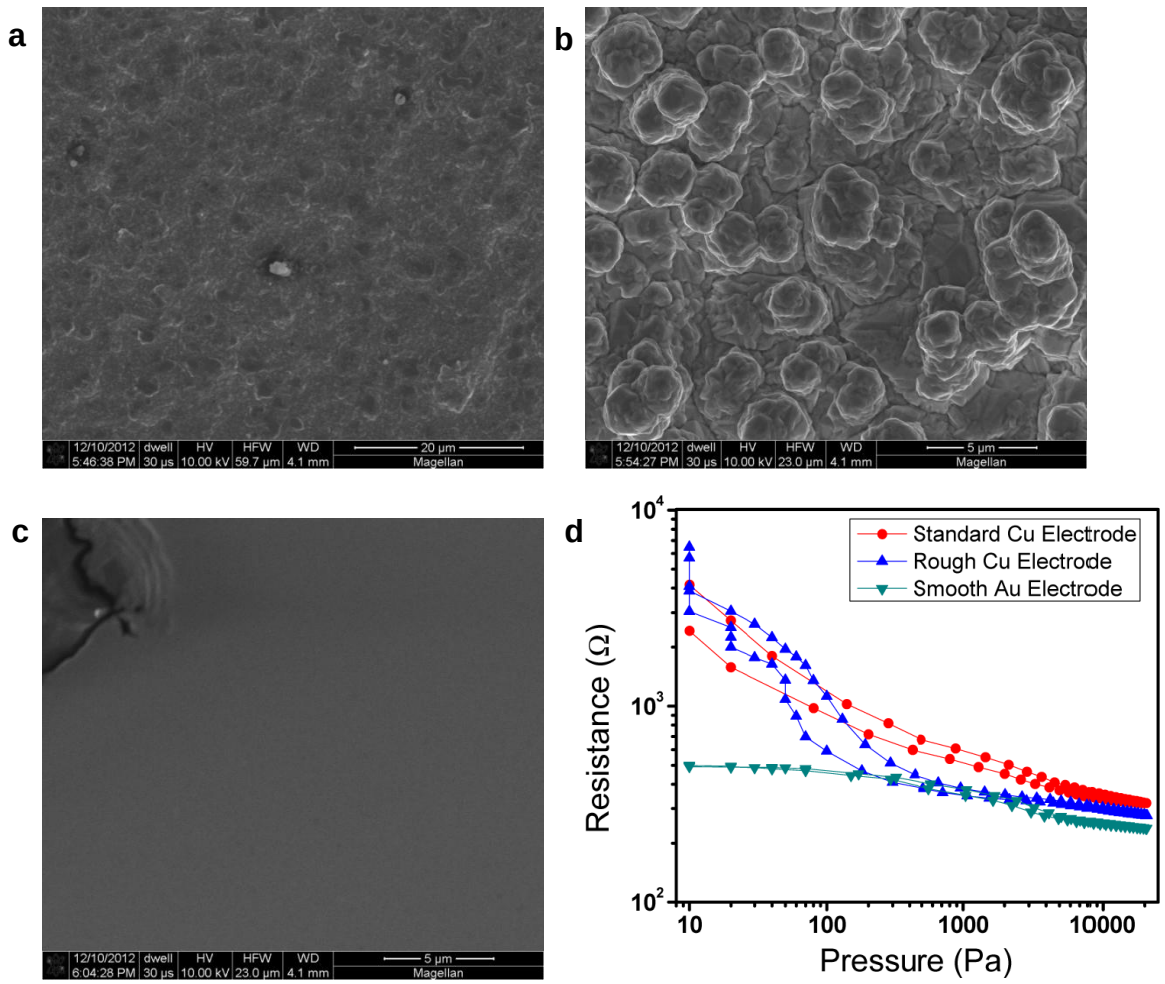

Supplementary Figure S11 | Effect of the electrode material and roughness. a, SEM image of the copper electrode used to characterize the PPy films in this publication. **b**, SEM image of a rough copper film used as an electrode. **c**, SEM image of a very smooth gold layer evaporated onto a thin polyimide layer. **d**, Pressure response curves of a microstructured PPy film with different top electrodes. The roughness and nature of the top electrode plays a very important role in determining the shape of the pressure response. Very little response was observed when the film was tested with the smooth gold electrode, and significant differences in shape were observed for the two different copper electrodes.

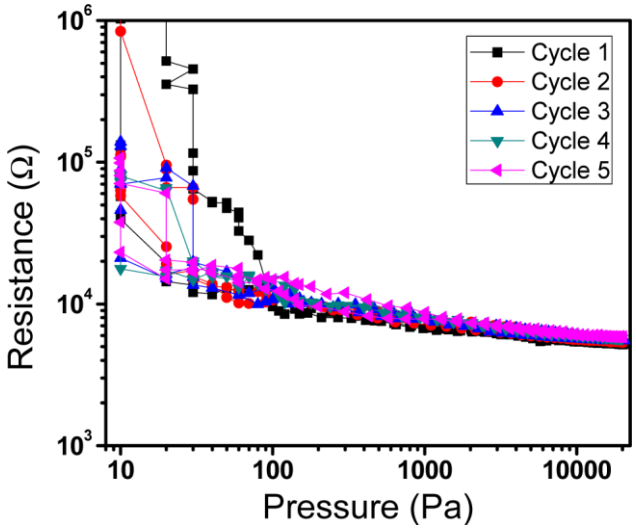

Supplementary Figure S12 | Resistance vs. pressure in the control material. PPy film synthesized using n-butanol. As shown in Fig. S5c, the film is composed of agglomerates of solid particles of PPy. Due to the lack of elastic microspheres, the device shows very little pressure sensitivity and displays irreproducible resistance values at low pressures.

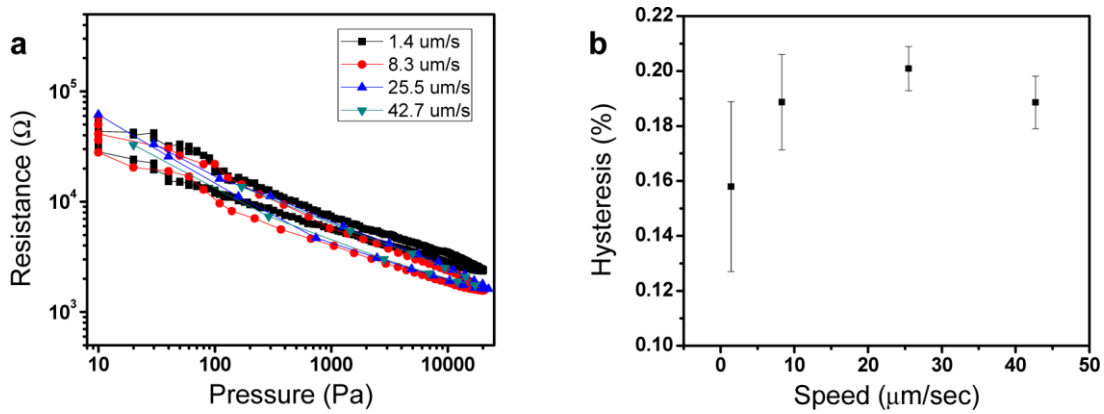

Supplementary Figure S13 | Pressure sensing as a function of loading speed. a, Resistance vs. pressure curves for the dry microstructured film at different loading speeds. **b,** Hysteresis in the resistance at different loading speeds. Hysteresis was defined as the maximum discrepancy between the loading and unloading curves divided by the full-scale output. On average, the hysteresis is lower during slower loading, as is commonly observed in mechanical testing. At speeds of 8.3 m/s and greater, the resistance vs. pressure curves were very similar.

Stability Testing

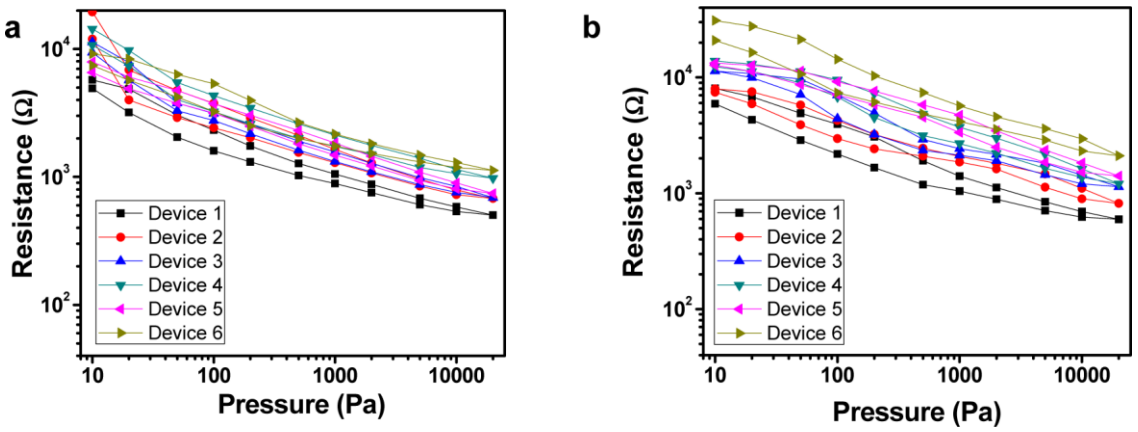

Supplementary Figure S14 | Reproducibility and temporal stability of six different devices. a, Resistance vs. pressure curves of six different devices. b, Resistance vs. pressure curves of the same six devices tested after 10 months of storage under ambient atmosphere. All devices were made with EMCP cut from the same film.

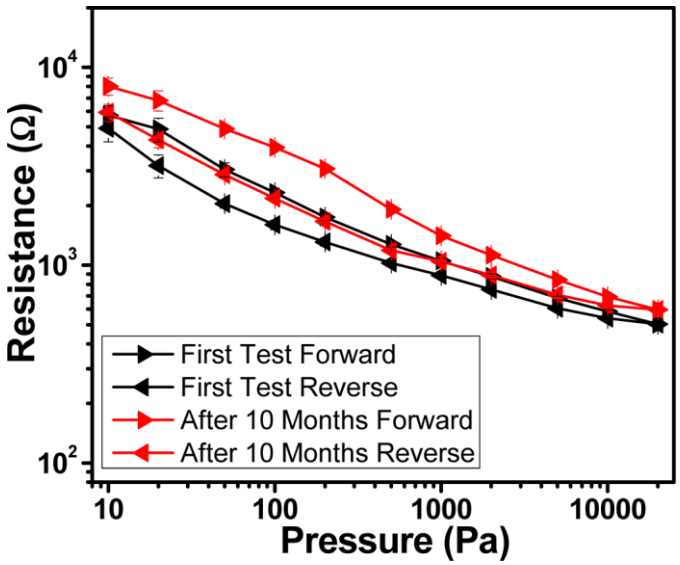

Supplementary Figure S15 | Comparison of sensing properties of one device before and after 10 months stored in dark and ambient condition. To investigate the shelf life of our material, we re-tested six devices after the EMCP thin films were stored in dark and ambient condition for ten months. The original measurements (Fig. S12a) and the measurements after 10 months (Fig. S12b) show resistance values that are qualitatively similar, although the spread in resistance values increased. As an example, the resistance vs. pressure data of a same device before and after storage is compared in Fig. S13. The increase in resistance showed an average increase in resistance of 77% (Fig.S12). Our phytic acid doped PPy showed good stability over time. In contrast, a dramatic increase in resistance of PPy with time has been observed in other reports, and is accelerated by exposure to air[42,63]. In ambient condition, the resistivity of the PPy increased by 3 to 5 times after one month[63,64]. In contrast, our EMCP film exhibited a much smaller change over a much larger timeframe, which we attribute to the stability of the crosslinking phytic acid dopant. The device stability should be further enhanced by improved encapsulation method and using more chemically stable electrodes.

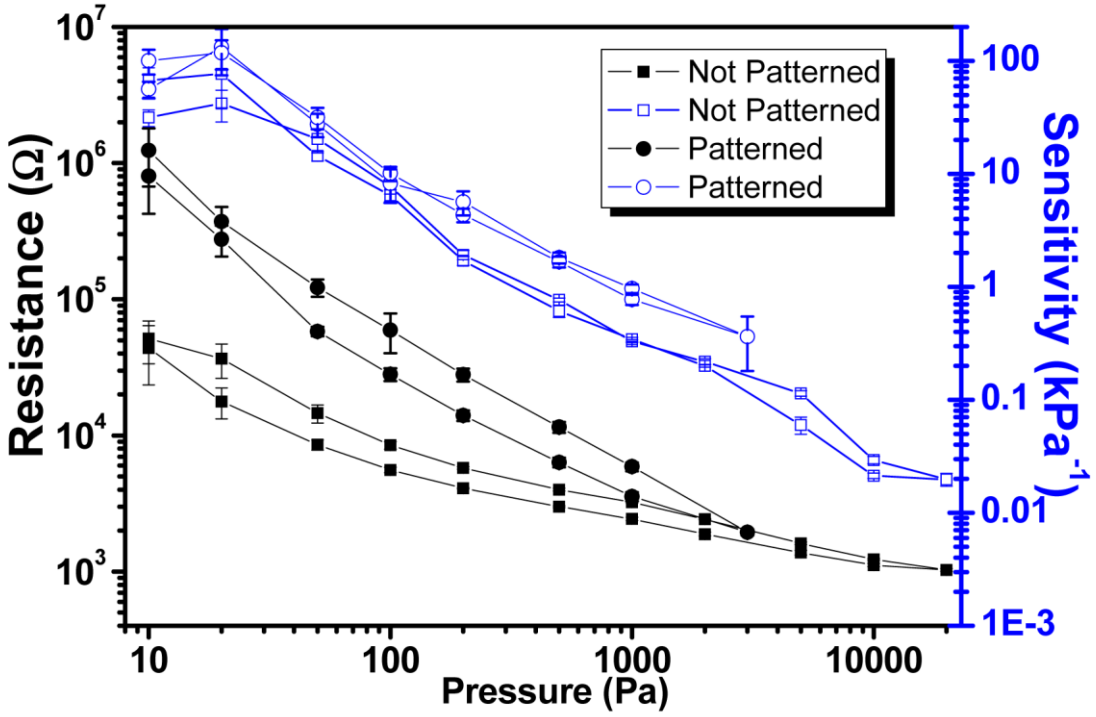

Supplementary Figure S16 |Sensing performance comparison between patterned and non-patterned PPy films. The patterned PPy film was prepared by casting the mixed precursor solution onto a PDMS mold with embossment of 1-mm period and 0.5-mm height cuniform embossment.

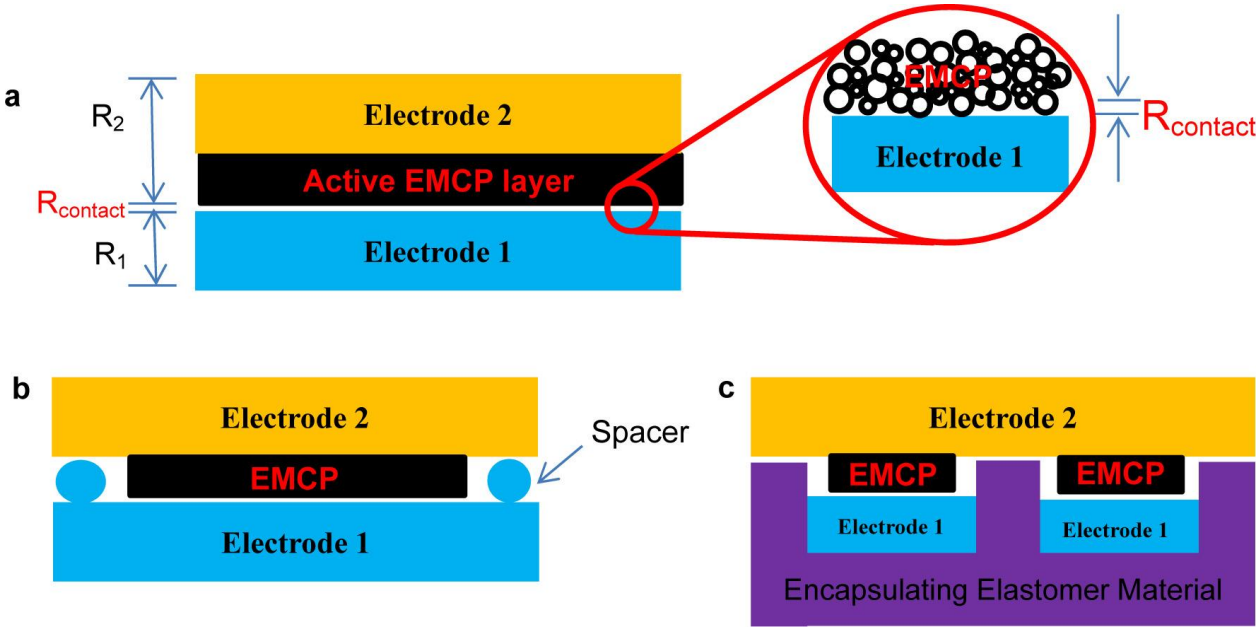

Supplementary Figure S17 | Structures for devices based on contact resistance. a, The illustrated schematic of the pressure sensor based on contact resistance working mechanism. **b**, Using a spacer to eliminate the preloaded pressure in device assembly. **c**, A well-structured encapsulating device structure to eliminate preloaded forces.

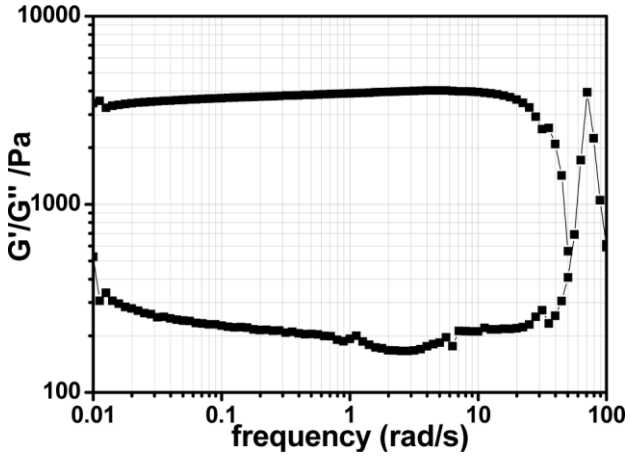

Supplementary Figure S18 | Dynamic frequency sweep of the wet PPy hydrogel at a strain of 1% at room temperature showed a typical hydrogel rheology behavior.

Supplementary Table S1. The calibrated weights of pieces measured by the pressure sensor array on a chess board.

Pixel Position	Chess piece	Color of piece	Measured Weight (g)	Real Weight (g)
A3	Pawn	White	1.881	1.995
D4	Pawn	White	1.993	1.920
F3	Pawn	White	1.979	1.920
G4	Queen	White	5.475	5.854
H4	Pawn	White	1.839	1.912
B5	Pawn	Black	3.582	3.589
D5	Pawn	Black	3.627	3.875
E6	Queen	Black	7.020	7.522
G6	Pawn	Black	3.720	3.875
H6	Pawn	Black	3.652	3.875

Supplementary Note 1

Confirmation of the Pressure Response Mechanism. A common method of eliminating contact resistance involves applying a conductive adhesive, such as silver paint or carbon black-loaded epoxy, between the test material and the electrode. However, because the EMCP is both hydrophilic and oleophyllic, conductive adhesives penetrated through the film, shorting the device. Consequently, a bottom-contact device geometry was used to confirm the mechanism of action. The EMCP placed on top of gold contacts displayed a change in resistance of several orders of magnitude with the application of pressure. The EMCP was then adhered to the gold electrodes by fully hydrating the material and then evaporating the water at 60 ℃. The process of rehydrating and then drying the material was used to improve both adhesion and electrical contact. The device was subsequently tested in the dry state. The resulting structure displayed no pressure response, indicating that the adhesion process eliminated the contact resistance and the pressure response. In the sandwich geometry, the pressure response was tested with and without adhering the film to the bottom gold electrode. The magnitude of the change in resistance with pressure was similar in both cases, indicating that the resistance originates at the contact between the EMCP and upper (non-adhered) electrode.

To confirm the piezoresistance mechanism, we utilized devices with "bottom contact" geometry (Supplementary Fig. S10a), in which both of the electrodes were below the PPy film. The operation of the devices with and without contact resistance was compared. When the EMCP film was placed on the electrodes, a large change in resistance was observed with increasing pressure, as shown in Supplementary Fig. S10b. However, after the contact resistance was eliminated by adhering the EMCP film to the electrodes through a wetting and heat treatment process, the resistance was effectively constant with applied pressure (Supplementary Fig. S10b). Therefore, the piezoresistance can be attributed to the contact resistance between the interfaces of the EMCP film and the electrode. This observation is consistent with previous research, which showed that PPy displayed little bulk piezoresistance[42,67].

In addition to the standard copper electrode, tests were conducted on the same PPy film with a very rough copper electrode and a smooth gold electrode. The standard and rough copper electrodes demonstrated a similar magnitude of contact resistance but different shapes of the pressure response. There was very little contact resistance between the smooth gold electrode and the PPy film and consequently very little pressure response as shown as Fig. S11. To investigate the importance of the microstructuring, bare ITO and a PPy film of solid particles were used as controls, as presented in Fig. S11d. As expected, the bare ITO showed no pressure response. The pressure response for the PPy film of solid particles was minimal, and the measured resistance was very noisy at low

pressures. Thus, the microstructure of both the film and the electrode are important in realizing the desired performance of the sensor.

Supplementary References

62 Oaki, Y., Kijima, M. & Imai, H. Synthesis and Morphogenesis of Organic Polymer Materials with Hierarchical Structures in Biominerals. *J. Am. Chem. Soc.* **133**, 8594-8599 (2011).

63 Wu, J., Zhou, D., Too, C. O. & Wallace, G. G. Conducting polymer coated lycra. *Synth. Met.* **155**, 698-701 (2005).

64 Hillis, W. D. A high-resolution imaging touch sensor. *Int. J. Robot. Res.* **1**, 33-44 (1982).